Effects of Oxide Roughness at Metal-Oxide Interface: MgO on Ag(001)

Sanliang Ling†, Matthew B. Watkins†, and Alexander L. Shluger†‡

† Department of Physics and Astronomy, University College London, Gower Street, London WC1E 6BT, United Kingdom

‡ London Centre for Nanotechnology, University College London, 17-19 Gordon Street, London WC1H 0AH, United Kingdom

E-mail: S.Ling@ucl.ac.uk

Abstract

Defects in thin oxide films on metal substrates affect metal work function and determine the chemical and physical properties of an oxide. However, accurately predicting properties of these heterogeneous systems is still challenging. Here we use a new approach to treat a mixed metal/metal oxide system within density functional theory, which is based on the application of the auxiliary density matrix method [*J. Chem. Theory and Comput.* **2010**, *6*, 2348] to calculate the exchange interaction at a sharp interface between the two materials, as implemented in the CP2K code. This method is used to calculate the shift of the Ag work function in MgO/Ag(001)

system as a function of the MgO film morphology as well as charge state, position and density of oxygen vacancies. An accurate band alignment between metal and oxide allows us to predict the relative stabilities of different charge states of oxygen vacancies in MgO as a function of their position with respect to the interface with Ag. Our results confirm that F^+ centers are the most stable defects at terrace sites of MgO clusters and show that F^0 and F^+ centres can have comparable energies at low-coordinated sites, such as steps and corners. They show how thin oxide film roughness as well as oxygen deficiency can affect the metal work function.

1. Introduction

Interfaces between metals and metal oxides are ubiquitous in nature and technology. Metal oxides are used to host metal nanoclusters in heterogeneous catalysis,[1] as substrates for metal nanoparticle deposition,[2] and in microelectronic devices.[3] Thin oxide films on well-defined metal surfaces form hybrid systems with applications in novel electronic and magnetic devices, chemical sensors, and as functional coating systems.[4] The interaction between metal oxide and metal substrate affects both the geometrical and electronic structures of oxide film and its performance in devices. For example, the property of metal oxide films to modify work function (WF) of metal substrates has been studied extensively both experimentally[5-8] and theoretically.[9-12] The two main contributions to the change of metal work function include compressive electrostatic effect and charge transfer at the interface.[10] The first contribution originates from Pauli's pushback effect, that the electron density which spills out of the metal surface is pushed back into the metal by the metal oxide thin film due to the Pauli repulsion. This decreases the surface dipole and thus the metal WF. The second contribution involves electron transfer across the interface. Such a transfer from the metal to the metal oxide thin film creates a dipole towards the metal and increases metal WF and *mutatis mutandis*.[13] Charged defects in the oxide film can further affect the metal WF.[4]

Thin, 2-4 monolayer oxide films are often rough and consist of metal oxide islands separated by metal patches.[14, 15] Experimentally, the shift of the metal WF induced by a dielectric thin film can be measured by different techniques,[14-19] such as Kelvin probe microscopy, scanning tunneling microscopy (STM) and field emission resonance (FER), all of which average the WF over a surface area of at least several hundred nm^2.[6] Most of the previous studies discussed the mechanism of metal work function shift induced by a thin layer of dielectric films based on ideal

slab models. In this paper we will focus on other factors affecting experimentally measured shifts of metal work function, such as roughness and defectiveness of the oxide film. An insight into how these factors can affect metal WF could help to achieve better control over the electronic properties of interfaces and allow them to be tuned as desired.

As an example we have chosen a relatively simple and well-studied system, MgO/Ag(001), the properties of which have recently been reviewed in detail.[20] STM experiments[15, 21] demonstrate that Ag islands appear alongside MgO clusters in the thin (2-4 MgO layer) film samples. The experimentally measured shift of the WF, $\Delta\phi$, for MgO/Ag(001) depends on both film preparation and method of WF measurement. For example, König *et al.* used Kelvin probe, STM and FER to measure $\Delta\phi$ of the same MgO/Ag(001) sample[6] and obtained $\Delta\phi$ values ranging between 1.1 eV for Kelvin probe to 1.4 eV for STM and FER. On the other hand, Jaouen *et al.* used ultraviolet photoemission spectroscopy to measure $\Delta\phi$ of the MgO/Ag(001) samples prepared under different conditions of oxygen partial pressure and sample temperature and found that the measured $\Delta\phi$ can vary by as much as 0.7 eV.[8] Therefore we compare a continuous film model to ones with different densities of MgO clusters on Ag(001) and study the effect of O vacancies with zero, one and two trapped electrons (otherwise called F-centers) in both MgO films and MgO clusters on the metal WF. We also determine the relative stabilities of different charge states of O vacancies (labeled F^0, F^+, F^{2+} when containing two, one or zero electrons, respectively) in thin MgO films supported on Ag(001). Calculating the relative stabilities has previously been complicated by the fact that the energy levels of F and F^+ centers in the band gap of MgO are predicted to be very close to the Fermi level of Ag.[22]

To address these issues one needs to obtain a correct band offset at the interface - the relative positions of the top of the valence band and of the bottom of the conduction band of MgO with

respect to the Fermi level of Ag. Calculating these energies using density functional theory (DFT) is still challenging as this requires a method which gives accurate predictions of the interface structure as well as the band gap of MgO and the Fermi level of Ag. Previously, Pacchioni *et al.* determined the energy levels of F centers from both embedded cluster calculations of MgO at hybrid DFT level with B3LYP functional[23] and periodic slab calculations of MgO/Ag(001) interface at generalized gradient approximation (GGA) level with PW91 and PBE functional.[22] While embedded cluster calculations with hybrid functionals give relatively accurate MgO band gaps,[24, 25] currently there is no effective embedding scheme for an interface system like MgO/Ag(001) to determine the energy levels of F centers with respect to the Ag Fermi level in the same calculation. On the other hand, periodic GGA calculations accurately predict the position of the Fermi level of Ag, but systematically underestimate the band gap of MgO by more than 2 eV,[24, 25] and the valence band offset by more than 1 eV. This means that the relative positions of F center states and the Ag Fermi level obtained from periodic GGA calculations of MgO/Ag(001) interfaces may prove unreliable. Hence, for more accurate predictions one ideally needs a method that gives an equally good description of both metal and oxide.

In this paper, we used a partitioning of the system based on the auxiliary density matrix method (ADMM)[26] implemented in the recent version of the CP2K code.[27] This method allows us to treat the metal at GGA level and the oxide at hybrid DFT level within the same calculation of the MgO/Ag(001) interface model. The efficiency of this approach, and of the underlying CP2K code, allow us to investigate large irregular systems such as MgO clusters on silver. The paper is organized as follows. In Section 2 we describe our methods and compare the performance of our approach with GGA and hybrid DFT on several important parameters, such

as lattice constant, metal WF and metal oxide band gap. In Section 3, we present our results on the shift of the WF of Ag(001) as a function of MgO film roughness and presence of oxygen vacancies and consider the effect of under-coordinated sites at cluster edges and corners; and in Section 4, we provide discussion and conclusions.

2. Methods

All calculations in this study are performed using the CP2K code,[27] which uses Gaussian basis set complemented by an auxiliary plane wave basis.[28] We used a double-ζ polarization quality Gaussian basis sets (DZVP-MOLOPT-SR-GTH) and a 350 Ry plane wave cutoff for the auxiliary grid.[28] PBE and PBE0 density functionals were used as described below, the hybrid PBE0 functional containing the original 25% of Hartree Fock exchange.

Calculations were performed using a periodic model in the Γ point approximation. In order to compensate for the lack of *k*-point sampling, 4x4x4 and 3x3x3 supercells were constructed for bulk Ag and MgO. We used a 3 layer 4x4 Ag periodic cell in a slab model to calculate the work function of the Ag(001) surface, and a 4 layer 4x4 periodic cell in a slab model to position the valence band maximum of MgO. For calculation of the WF and Schottky barrier height of the MgO/Ag(001) interface, both MgO clusters and continuous MgO films on Ag(001) were also simulated in a slab model (including 2D electrostatics[29]). MgO clusters and slabs with thicknesses of 3 and 4 layers were calculated and no significant difference in the change of WF was found. In most calculations of MgO on the Ag(001) surface we used a 4x4 periodic cell for both MgO and Ag, both of which had a thickness of 3 layers. Three layers of Ag were sufficient to converge the metal work function, the primary property of interest here. To model different MgO coverages, we placed 3x3, 4x4 or 5x5 MgO clusters on top of a 6x6 Ag(001) periodic cell.

For all interface calculations MgO is forced to take the lattice parameter of Ag in the initial structure, with O atoms positioned above Ag atoms and Mg atoms at the hollow site.

Geometry optimization of the MgO/Ag(001) interface was performed using the PBE functional, with the bottom layer of Ag fixed. These geometries were used for single point energy calculations of WF shifts. The work function (ϕ) of Ag and the effective work function of MgO/Ag(001) interface are defined as the energy difference between the Fermi level and the vacuum level, which is determined as the self-consistent electrostatic potential in the vacuum. The shift of the work function ($\Delta\phi$) is defined as $\Delta\phi = \phi(\text{Ag}) - \phi(\text{MgO/Ag})$. The Schottky barrier height (E_{SB}) is defined as the difference between the Fermi level and the top of the valence band of MgO, both of which were determined for the interface system.

To choose a calculation scheme we used the following considerations: Periodic GGA calculations with PBE in CP2K are very fast and give accurate lattice parameters for Ag and MgO, as well as WF of Ag compared with the experimental values.[9] However, they underestimate the band gap and ionisation potential (IP) of MgO by more than 2 eV (see Table 1). On the other hand, periodic calculations with a hybrid functional, PBE0, give similarly good WF of Ag and much better band gap and IP of MgO, but are much slower and require a lot of memory, due to the fact that a brute force calculation of Hartree-Fock exchange interaction (HFX)[26] scales as $O(N^4)$. The use of hybrid functionals on metallic systems is also known to degrade the cohesive energy of the metal, severely distort band structure, and lead to qualitatively incorrect screening[24] within the metal, though these limitations do not appear to manifest themselves on the properties of direct interest here. To obtain a correct band offset of the MgO/Ag(001) interface at a reasonable computational cost, the best choice would be to use PBE for Ag and a related hybrid functional (PBE0) for MgO. This is not feasible for most of the

available periodic DFT codes. However, recent implementation of ADMM method[26] in CP2K code in principle allows one to use different methods for different atoms in a combined system through using different auxiliary basis sets for calculating HFX in different parts of the system.

As a method initially designed to accelerate HFX calculations, ADMM works by exploiting the different interaction range of Hartree-Fock exchange from that of the underlying GGA functional in a hybrid DFT calculation. A good quality primary basis-set (e.g. MOLOPT basis set[28]) is used for the GGA calculation, but is approximated by that of an auxiliary basis set, which is much smaller in terms of size and spatial extent, for the calculation of the HFX term. To improve the approximation, a correction term of the difference in exchange energy of the GGA functional between the primary and auxiliary basis sets is applied. The hope is that this difference in Hartree-Fock exchange energy with change of basis set is well accounted for by the GGA exchange functional.

There is considerable flexibility in how to construct auxiliary basis sets, depending on specific systems.[26] We opt to use three Gaussian exponents on each valence orbital (FIT3) optimized in atomic calculations. This approximation was shown to give good results for a variety of systems including the GMTKN24 Database[26] and behaves similarly well for MgO, see Table 1. In its simplest form, the auxiliary density matrix is formed by projecting the Kohn-Sham orbitals of the primary basis-set onto the auxiliary. More sophisticated methods restore the idempotency (or equivalently the orthonormality of the auxiliary Kohn-Sham orbitals) of the formed auxiliary density matrix. By using the known projectors connecting the two density matrices ($\mathbf{P}_{\text{primary}}$, $\mathbf{P}_{\text{auxiliary}}$), it is possible to form the complete Kohn-Sham matrix, **K**, for the system from the energy,

$$E_{total} = E[\boldsymbol{P}_{primary}] + E[\boldsymbol{P}_{auxiliary}],$$

$$\boldsymbol{K} = \boldsymbol{K}_{primary} + \frac{dE[\boldsymbol{P}_{auxiliary}]}{d\boldsymbol{P}_{primary}},$$

and carry out self-consistent calculations in the normal manner.

The use of the ADMM method not only accelerates HFX calculations in CP2K, but also provides an additional degree of control over the computational procedure, which one can exploit. For example, we can construct different auxiliary basis sets for different atoms in a system, so that different amounts of HFX are calculated for different atoms. In the case of MgO on Ag(001), we can use FIT3 auxiliary basis-set for MgO and another auxiliary basis-set for Ag. As mentioned earlier, a preferable choice would be to treat Ag with just PBE, i.e. with zero percent of HFX mixed into the functional. To do this, we designed an auxiliary basis set for Ag with only one Gaussian exponent for each Ag atom and denote this auxiliary basis set as MIN. In this way, there is almost no contribution to the auxiliary density matrix from Ag atoms, which effectively results in using the PBE functional for the Ag part of the system. Note that recently an approach has been reported with the WIEN2k code,[30] in which the exact exchange is only applied for selected atomic orbitals inside given atomic spheres.

In very rare situations we impose PBE0 on Ag, in which we would have to use an aug-FIT3 quality[26] auxiliary basis set (3 Gaussian exponents on each valence orbital plus augmented diffuse functions, which leads to a total of 9 exponents on each Ag atom) due to the extended nature of Ag charge density in a metallic environment. Such calculations are very time-consuming and not feasible for the extensive studies required here. This prohibitive computational cost to accurately calculate HFX in the metal is a further motivation for the mixed functional approach adopted here. For all calculations involving metallic Ag, Fermi-Dirac smearing is used with an electronic temperature of 3000 K to accelerate convergence to self-consistency.

3. Results of Calculations

3.1 Shift of the Ag work function: perfect MgO slab

The calculated values of ϕ and $\Delta\phi$ for the perfect MgO/Ag(001) slab are compared with the results of previous calculations and with experimental values in Table 2. While previous calculations for $\Delta\phi$ using plane wave and PW91 functional give very good agreement with experiment, our calculations based on localised basis sets show a much bigger discrepancy. One can see that all three theoretical methods, i.e. PBE and PBE0 for the whole interface, and PBE0 for MgO and PBE for Ag, overestimate $\Delta\phi$ by about 0.4 eV or more, compared with the experimental values. The reason is that, compared to the previous theoretical calculations using a plane-wave basis set, in which the distance between MgO and Ag was 2.73 Å,[9] our PBE optimized interface distance is smaller, 2.58 Å. An even smaller distance of 2.53 Å has been reported in another theoretical study using a localized basis set,[31] while the experimentally reported interface distances for MgO/Ag(001) and Ag/MgO(001) vary between 2.39 and 2.53 Å.[21, 32, 33] Therefore our results are, in fact, in better agreement with available experimental structural data than the plane wave calculations.

To understand the reasons behind this, we carried out geometry optimizations using CP2K and the plane-wave VASP code,[34] using both GGA and GGA with empirical dispersion corrections. The VASP PBE calculations using plane-wave basis sets are in agreement with the literature[9] with an Ag-O distance of 2.70 Å, but the inclusion of Grimme's D2 dispersion correction[35] led to a significant reduction of Ag–O distance to 2.50 Å. The combination of PBE+D2 with Mg cations is likely to overestimate the dispersion interaction here.[36] Indeed, the inclusion of Grimme's most recent D3 correction,[37] which is less empirical and provides better description to dispersion interaction than the D2 correction that overestimates midrange dispersion, gives an

Ag-O distance of 2.62 Å. Although these calculations were carried out with fixed geometry within Ag and MgO layers, they clearly demonstrate the importance of the dispersion correction.

The full geometry optimization in CP2K PBE calculation with the D2 correction led to reduction in the interface Ag-O distance - from 2.58 Å to 2.49 Å. However, the inclusion of the D3 correction,[37] gives almost the same interface Ag–O distance as that obtained without any empirical dispersion correction – at the 2.58 Å separation the D3 dispersion force is too week to change the MgO – Ag(001) distance. The difference between PBE, PBE-D2 and PBE-D3 suggests that using localized basis-sets we fortuitously arrived at a good agreement with the experimentally measured Ag – MgO distance through basis set superposition error mimicking the missing dispersion interactions. The basis sets we used give excellent properties for the individual materials, but the weak interfacial interaction here is a challenging test to describe accurately using such functions. The situation would be less severe in more strongly interacting systems.

The shorter interface distance means a larger compression of the electron density in Ag, which results in a more pronounced reduction of the work function (in both plane wave and local basis set calculations), which is the main reason why our $\Delta\phi$ value is bigger than previous theoretical value[10] by about 0.5 eV. To further confirm that our larger $\Delta\phi$ value is mainly due to a shorter interface distance, we calculated $\Delta\phi$ based on a bigger interface distance, e.g. 2.78 Å (compared with 2.73 Å in Ref. 9) and obtained 1.4 eV, which is close to that reported in Ref. 9 (1.2 eV).

3.2 Shift of the work function: MgO islands

As mentioned earlier, the experimentally measured $\Delta\phi$ is averaged over the probe area, and hence, depending on the size of the probe, different areas are used for averaging. For example,

the radius of averaging area of Kelvin probe measurements is about 15-30 nm,[6] which is larger than the typical size of MgO islands in these experiments. This means that, if the experimental $\Delta\phi$ averages over MgO islands and patches of bare Ag(001) surface, it might be smaller than the shift from a perfect MgO film.

To mimic incomplete coverage, we considered MgO clusters on top of the Ag(001) substrate. This has an added benefit as optimizing the geometry of a cluster allows one to release the strain due to the lattice mismatch between MgO and Ag(001), which is otherwise present in the slab calculations. To simulate different coverages, we consider 3x3, 4x4 and 5x5 MgO clusters on top of a 6x6 Ag(001) periodic cell (see Figure 1). This corresponds to coverages of 17%, 34% and 56%, respectively. We note that the corresponding periodic cells include up to 324, 408 and 516 atoms, respectively, and such calculations are currently feasible only due to the efficient hybrid scheme described above.

The calculated $\Delta\phi$ values for different coverages of MgO on Ag(001) are summarized in Table 3, where we also include the data for the perfect MgO slab (100% coverage) for comparison. One can see that $\Delta\phi$ increases roughly linearly with the MgO coverage, and for an MgO cluster covering 56% of the surface area of Ag(001), our calculated $\Delta\phi$ is within the range of experimental values. This suggests that in some of the measurements the samples either exhibit only partial coverage, or there exist interface/electron trapping sites affecting $\Delta\phi$ that have not yet been identified.

In Table 3, we also list the average Ag-O distances at the interface for Ag(001) surface with different MgO coverage. One can see that the interface distance increases with the MgO coverage due to increased strain energy. The shorter interface distance results in a more

pronounced reduction of the WF and deviation from linearity with coverage, however, this is a less important factor than the coverage change itself.

3.3 Relative stabilities of F centers

Oxygen vacancies or F centers can be present in MgO films either as a result of film preparation or irradiation by photons or electrons.[23] It has been suggested that positively charged F centers can shift the local potential,[6] and that electron trapping at surface F centers increases local electron densities above the surface.[6] Both of these effects will affect the shift of the Ag(001) work function. Since the experimentally measured shift of the work function is an averaged property, it will depend on the location, density and charge state of point defects present in the MgO film. In principle, F centers at different positions in MgO islands, e.g. in the surface/middle/interface layers of MgO, or at terrace/corner/kink sites (see Figure 4), may have different effects on the shift of the metal WF. To understand how the presence of F centers affects the experimentally measured $\Delta\phi$, it is thus necessary to determine the relative stabilities of their charge states in different locations within MgO islands.

The geometric and electronic structures of F centers at surfaces of isolated MgO nanoclusters and in MgO films on Ag(001) have already been studied in a number of publications (see e.g. Refs. 22 and 38, and Ref. 20 for recent review). The displacements of the nearest neighbor ions in different charge states of an F center follow the order $F^0 < F^+ < F^{2+}$, see Figure 2b. The GGA calculations[22] have demonstrated that the charge state of F centers in MgO films is determined by a subtle interplay between the position of defect states with respect to the metal Fermi level and defect-induced lattice relaxation (polaronic effect) as a function of the defect position in the MgO slab. Here we investigate this effect further.

Due to technical limitations, we are unable to routinely optimize the whole interface structure using our hybrid PBE/PBE0 scheme. Therefore, we used the following approach. First, we optimize the whole stoichiometric interface structure (either MgO slab or MgO cluster on the Ag(001) substrate) without any defect with PBE. Then we fix the interface layer of MgO, create an O vacancy in different layers (surface, second, and third, for the case when we have an MgO cluster with four layers) and at different positions in MgO clusters, and optimize the geometry of different charge states of an F center in an *isolated* (unsupported) MgO slab/cluster with PBE0. Finally, we put the optimized MgO clusters back on to the Ag(001) substrate, using the same positions and interface distances obtained from PBE geometry optimizations, and calculate the electronic structure of the whole interface with the mixed PBE/PBE0 method.

We stress that the total number of electrons in each MgO/Ag(001) system considered remains constant independent of the F center charge state and corresponds to two electrons in the oxygen vacancy. Thus the overall system is neutral and no special precautions are needed to deal with the electrostatics. However, electron transfer into Ag may cause less than two electrons to occupy the defect in the combined interface system. The amount of electron transfer can be controlled by distorting the local geometry around a defect in the correspondence with a desired charge state. This allows a direct comparison of the *total energies* of the system in different defect charge states.

To construct potential energy surfaces (PESs) for MgO/Ag(001) systems with F centers in different charge states with respect to the configuration coordinate representing displacements of all surrounding ions, we use atomic configurations obtained by interpolation between each pair of F^0/F^+ and F^+/F^{2+} centers using their respective geometries optimized in an isolated MgO cluster (see Figure 2b), and then perform single point energy calculations at PBE/PBE0 level for

each point. For example, there is negligible distortion of surrounding ions around the F^0 center in the second MgO layer. However, the nearest neighbor Mg ions are displaced outwards by 7% of the interatomic distance around the F^+ center and by 13% around the F^{2+} center in the isolated MgO cluster (see Fig. 2b).

The PESs for F centers in the surface, as well as in the second and third layers of a 3x3 MgO(4L) cluster on a 6x6 Ag(001) slab are shown in Figure 2a. One can see that in all three cases, the total energy of the system with the F^+ center is lower than these with F^0 and F^{2+} centers by about 0.2-0.6 eV, indicating that the F^+ center is thermodynamically the most stable defect charge state in all three cases. However, the relative energy positions of the F^+ centers are shifted towards the F^0 center in the top layer of MgO, and towards the F^{2+} center in the second and third layers of MgO due to the interaction with the Ag(001) substrate. As one can see in Figure 2a, the minimum positions for F^0 and F^{2+} centers in the top and third layers of MgO are not very distinct, which most likely means very little electron transfer from/to Ag in these configurations with respect to the F^+ center. However, for the F^0 and F^{2+} centers in the second layer of MgO, there is a clear change in the energy gradient of the PES for the corresponding geometries, indicating a significant change in the defect charge state. We are thus able to calculate three separate potential energy curves (see dashed red lines in Figure 2a), corresponding to the lattice distortion around F^0, F^+ and F^{2+} centers. From the inter-crossing of these curves one can infer that the adiabatic transition barriers from F^0 and F^{2+} to F^+ centers are very low, which means that F^0 and F^{2+} centers are metastable even at low temperatures. An F^+ center in the surface layer of this MgO cluster is favoured over the F^+ centers in the second and third layers, the former being more stable than the latter by 0.3~0.4 eV.

Contrary to the terrace sites, the energies of F^0 and F^+ centers at the corner of the MgO(3x3) cluster on Ag(001) differ only by 0.02 eV, and are more stable than the F^{2+} center by more than 0.6 eV. However, F^0 centers at the cluster edge are more stable than F^+ centers by about 0.05 eV. To check how these results depend on the MgO cluster size, we have also considered the relative stabilities of F centers at different sites in a much bigger MgO(5x5) cluster on the Ag(001) slab (see Table 4). In this case F^0 centers are more stable than F^+ centers at terrace, corner and edge sites, with relative stabilities ranging from 0.05 eV to 0.16 eV. Although F^+ is still more stable than F^0 at a step-corner site, we find that the energy difference between F^+ and F^0 centers is reduced by half compared with that of a smaller MgO(3x3) cluster. However, at a kink site an F^+ center is more stable than an F^0 center by up to 0.4 eV. This difference between the corner and kink sites is caused by different local environment and relaxation of surrounding ions.

3.4 Shift of the work function: F centers

The WF change $\Delta\phi$ of Ag(001) resulting from the presence of F centers in MgO films depends on the combined effect of the charge state, density and position of F centers in the film. The results presented above demonstrate that F^+ centers are the most thermodynamically stable at terrace sites, F^0 and F^+ centers can co-exist at lower-coordinated corner and kink sites, but that F^{2+} centers are thermodynamically unstable at all sites we considered. The Kelvin probe microscopy data in Ref. 6 have been interpreted in terms of co-existence of all three defect charge states, with F^0 center found to be the most abundant (45%). Admittedly, the defect images presented are either at or close to the low-coordinated sites on MgO islands supported on Ag(001) substrate. Therefore the statistics behind the charge state abundance figures in Ref. 6 is not clear.

For completeness, we looked at the effect of all three defect charge states on the work function shift of Ag(001) as a function of defect position and density.

We start by calculating shifts of the work function for an MgO/Ag(001) in the 4x4 slab model with the surface F^0, F^+ and F^{2+} centers. To understand better the effect of defects at the interface, we calculated how the electron density redistributes when two separate Ag(001) and MgO slabs are put together to form an interface, with and without F centers present. The electron density differences are calculated between the perfect MgO(3L)/Ag(001) interface and the two separated components, a bare Ag(001) slab and an unsupported MgO slab and one with F^0, F^+, F^{2+} centers in the surface layer, with the geometries of isolated and combined systems being the same.

The introduction of a surface F^0 center in MgO changes $\Delta\phi$ very little compared to the perfect MgO slab on Ag(001). As one can see in Figure 3, the electron density differences for the perfect slab and the slab with the surface F^0 center are very similar, which explains this small change. On the other hand, positively charged surface F^+ or F^{2+} centers increase $\Delta\phi$ by about 0.71 eV and 1.21 eV, correspondingly, due to the local polarisation around the oxygen vacancy clearly seen in Figure 3. Note that the total number of electrons is conserved in Figure 3, which means that in comparison with the surface F^0 center, electron density is transferred from MgO into Ag substrate in the cases of the surface F^+ and F^{2+} centers. This results in the formation of a dipole layer towards MgO, reduction of the effective work function, and hence in further increase of $\Delta\phi$. It should also be pointed out that the electron density differences in the interface region are almost the same for all the four cases in Figure 3. This is due to the fact that the amount of electron transfer across the interface is still small compared to the total number of electrons in Ag (around 0.1%).

To find how the concentration of F centers will affect $\Delta\phi$, we compare the results for the 4x4 MgO/Ag(001) slab with that for the 6x6 slab where the defect density is about $1.6x10^{13}$ defects/cm^2, less than half of that of a 4x4 slab. As one can see in Table 5, the $\Delta\phi$ for the 6x6 slab is reduced to about half of that of a 4x4 slab, for both F^+ and F^{2+} centers. Finally, $\Delta\phi$ also depends on the actual positions of F centers in the MgO slab or in a surface island, e.g. on the distance to Ag substrate and the number of nearest neighbors. The $\Delta\phi$ values for F centers at different positions in an MgO cluster shown Figure 4 are summarized in Table 6. One can see that in most cases, for the same charge state, $\Delta\phi$ at different positions differ by less than 0.15 eV. This indicates that for three layers of MgO, the actual position of an F center is less important in determining $\Delta\phi$ than the charge state.

Finally, we note that at a relatively high coverage, e.g. 56%, of MgO on Ag(001), the adjacent periodic images of MgO clusters interact with each other. For example, an F center at a corner site might be affected by a dipole moment at an Mg corner at about 6 Å away in the next unit cell (see Figure 4). This effect proves to be still quite small for the properties discussed above. Taking F^+ center at a corner site as an example, for a 3x3 MgO cluster on a 6x6 Ag(001) slab, the energy levels of occupied and unoccupied states are 1.32 eV below and 0.54 eV above the Fermi level, respectively, and for the 5x5 MgO cluster on the 6x6 Ag(001) slab, the corresponding values are 1.37 eV and 0.50 eV, respectively.

4. Discussion and Conclusions

We have employed a novel computational scheme to allow efficient hybrid functional calculations in the solid state and to model a mixed metal/metal oxide system. This approach is based on using the ADMM[26] to evaluate the exchange interaction at a sharp interface between

the two materials, and is exploiting the flexibility allowed by localised basis sets to only calculate HFX for parts of the system of interest. It is applied to calculate the shift of the WF of Ag(001) as a function of the MgO film morphology as well as charge state, position and density of F centers. This efficient method allowed us to calculate large periodic cells with mixed PBE/PBE0 treatment of Ag and MgO, respectively. It should be pointed out here that such an approach works well for weakly interacting interface systems, e.g. MgO/Ag(001), and extra care should be taken when it is applied to strongly interacting interface systems.

For the perfect MgO/Ag(001) slab system we observe that the calculated Ag – MgO distance (all our interface geometries were obtained at GGA level) is much shorter than obtained by the plane-wave GGA calculations, but close to the experimental data from EXAFS.[32] Our calculations demonstrate that the discrepancy between the converged plane wave calculations and experiment is in this case likely to stem from the neglect of non-local dispersion interactions. For an interface with little charge transfer or covalent binding character these interactions can make a significant contribution to the adhesive energy and strongly affect metal/metal oxide distances.[39] We are investigating this effect in more detail, but feel confident that the geometries obtained in this paper and the consequent increase in the work-function shift compared to previous calculations are physical.

The $\Delta\phi$ obtained with this distance is significantly larger than that measured in different experiments made on rough MgO/Ag(001) systems with partial coverage of Ag(001) surface by MgO islands. We demonstrate that one can obtain a good agreement with the experimental values of $\Delta\phi$ at about 50-60% percent coverage of Ag(001) by three or four layer MgO islands. We also report on the stability of different charge states of the F centers on top of MgO terraces as well as inside MgO clusters.

To compare our results with those described in the discussion of STS measurements in Ref. 23, we have also calculated one-electron defect levels of oxygen vacancies at different positions in a 5x5 MgO cluster supported on a 6x6 Ag(001) slab (see Figure 5a). We note at this point that our calculations correspond to the constant number of electrons in the MgO/Ag(001) system and more accurate comparison to the STS measurements[23] would require a constant electron chemical potential treatment (see, for example, Ref. 40). The doubly occupied states of F^0 centers at most of the positions (except for a kink site) span a narrow range of 0.6~0.8 eV below the Fermi level. The singly occupied F^+ center states at most of the defect positions (except for a kink site) span a narrow range of 1.3~1.4 eV below the Fermi level, and the corresponding unoccupied states span a slightly wider range of 0.4~0.8 eV above the Fermi level. The occupied states of F^0 and F^+ centers at a kink site are shifted towards the Fermi level by about 0.3~0.4 eV: the defect level of an F^0 center is only 0.35 eV below the Fermi level, and the defect level of the occupied state of an F^+ center is 1.0 eV below the Fermi level.

Apart from the vacancy states, the under-coordinated cluster atoms also give rise to states in the MgO gap.[41] In particular, the occupied states of under-coordinated oxygen atoms at corner sites (see Figure 5b) have energy levels about 2.3~2.4 eV, for clusters with F^0 centers, and about 2.5~2.6 eV, for clusters with F^+ centers, below the Fermi level, respectively (see Figure 5a). We note that these states are mainly localised on specific under-coordinated oxygen atoms at corner sites but also spread over other under-coordinated oxygen atoms nearby (see Figure 5b). Therefore their energies are not very sensitive to the MgO cluster size. However, the presence of an F^+ center in the cluster shifts the energies of under-coordinated corner oxygen states down by about 0.2 eV, comparing with the F^0 center. Low coordinated sites of MgO nanoclusters, such as corners and kinks, have been shown to serve as electron traps.[41] However, in the case of the

MgO cluster on the Ag(001) substrate, we find that energies of extra electrons are much higher than the Ag Fermi level and corners and kinks are not stable electron traps.

To summarize, our ability to examine more realistic models of the MgO/Ag interface has been facilitated by both the efficient hybrid functional scheme within CP2K and our further approximation that neglects HFX within the metal. Using more sophisticated models and hybrid functionals in interface simulations will facilitate our understanding of these systems. We also re-raise the question of the importance of dispersion interactions in modelling the structure and properties of metal/metal oxide interfaces.

Acknowledgement

This work was supported by European FP7 MORDRED project. M. Watkins was supported by the Leverhulme Trust (grant F/07 134/CK). We would like to thank Joost VandeVondele for enlightening discussions about the ADMM method and Livia Giordano for discussions on properties of interfaces. We are grateful to Samuel Bradley for help in calculations. Via our membership of the UK's HPC Materials Chemistry Consortium, which is funded by EPSRC (EP/F067496), this work made use of the facilities of HECToR, the UK's national high-performance computing service, which is provided by UoE HPCx Ltd at the University of Edinburgh, Cray Inc and NAG Ltd, and funded by the Office of Science and Technology through EPSRC's High End Computing Programme.

References

1. Chambers, S. A., *Surf. Sci. Rep.* **2000,** *39*, 105-180.
2. Freund, H.-J.; Pacchioni, G., *Chem. Soc. Rev.* **2008,** *37* (10), 2224-2242.
3. Robertson, J., *J. Vac. Sci. Technol. B* **2009,** *27*, 277-285.

4. Netzer, F. P.; Allegretti, F.; Surnev, S., *J. Vac. Sci. Technol. B* **2010,** *28* (1), 1-16.

5. Greiner, M. T.; Chai, L.; Helander, M. G.; Tang, W.-M.; Lu, Z.-H., *Adv. Funct. Mater.* **2012,** *22* (21), 4557-4568.

6. König, T.; Simon, G. H.; Rust, H. P.; Heyde, M., *J. Phys. Chem. C* **2009,** *113* (26), 11301-11305.

7. Jaouen, T.; Jezequel, G.; Delhaye, G.; Lepine, B.; Turban, P.; Schieffer, P., *Appl. Phys. Lett.* **2010,** *97* (23), 232104.

8. Jaouen, T.; Jezequel, G.; Delhaye, G.; Lepine, B.; Turban, P.; Schieffer, P., *Appl. Phys. Lett.* **2012,** *100* (2), 022103.

9. Giordano, L.; Cinquini, F.; Pacchioni, G., *Phys. Rev. B* **2006,** *73*, 045414.

10. Prada, S.; Martinez, U.; Pacchioni, G., *Phys. Rev. B* **2008,** *78*, 235423.

11. Goniakowski, J.; Noguera, C., *Interface Sci.* **2004,** *12* (1), 93-103.

12. Sementa, L.; Barcaro, G.; Negreiros, F. R.; Thomas, I. O.; Netzer, F. P.; Ferrari, A. M.; Fortunelli, A., *J. Chem. Theory Comput.* **2012,** *8* (2), 629-638.

13. Goniakowski, J.; Mottet, C.; Noguera, C., *physica status solidi (b)* **2006,** *243* (11), 2516-2532.

14. Bieletzki, M.; Hynninen, T.; Soini, T. M.; Pivetta, M.; Henry, C. R.; Foster, A. S.; Esch, F.; Barth, C.; Heiz, U., *PCCP* **2010,** *12* (13), 3203-3209.

15. Ouvrard, A.; Niebauer, J.; Ghalgaoui, A.; Barth, C.; Henry, C. R.; Bourguignon, B., *J. Phys. Chem. C* **2011,** *115* (16), 8034-8041.

16. Barth, C.; Henry, C. R., *Appl. Phys. Lett.* **2006,** *89* (25), 252119.

17. Barth, C.; Henry, C. R., *J. Phys. Chem. C* **2009,** *113* (1), 247-253.

18. Baier, R.; Leendertz, C.; Lux-Steiner, M.; Sadewasser, S., *Phys. Rev. B* **2012,** *85* (16), 165436.

19. Sadewasser, S.; Jelinek, P.; Fang, C.-K.; Custance, O.; Yamada, Y.; Sugimoto, Y.; Abe, M.; Morita, S., *Phys. Rev. Lett.* **2009,** *103* (26).

20. Pacchioni, G.; Freund, H., *Chem. Rev.* **2012**, DOI: 10.1021/cr3002017.

21. Giovanardi, C.; di Bona, A.; Moia, T. S.; Valeri, S.; Pisani, C.; Sgroi, M.; Busso, M., *Surf. Sci.* **2002,** *505* (0), L209-L214.

22. Giordano, L.; Martinez, U.; Pacchioni, G.; Watkins, M.; Shluger, A. L., *J. Phys. Chem. C* **2008,** *112*, 3857-3865.

23. Sterrer, M.; Fischbach, E.; Heyde, M.; Nilius, N.; Rust, H. P.; Risse, T.; Freund, H. J., *J. Phys. Chem. B* **2006,** *110*, 8665-8669.

24. Paier, J.; Marsman, M.; Hummer, K.; Kresse, G.; Gerber, I. C.; Angyan, J. G., *J. Chem. Phys.* **2006,** *124*, 154709.

25. Clark, S. J.; Robertson, J., *Phys. Rev. B* **2010,** *82*, 85208.

26. Guidon, M.; Hutter, J.; VandeVondele, J., *J. Chem. Theory Comput.* **2010,** *6*, 2348-2364.

27. VandeVondele, J.; Krack, M.; Mohamed, F.; Parrinello, M.; Chassaing, T.; Hutter, J., *Comput. Phys. Commun.* **2005,** *167*, 103-128.

28. VandeVondele, J.; Hutter, J., *J. Chem. Phys.* **2007,** *127* (11), 114105.

29. Genovese, L.; Deutsch, T.; Goedecker, S., *J. Chem. Phys.* **2007,** *127* (5), 054704.

30. Zhang, Y.; Castets, A.; Carlier, D.; Ménétrier, M.; Boucher, F., *J. Phys. Chem. C* **2012,** *116* (33), 17393-17402.

31. Ferrari, A. M., *Surf. Sci.* **2005,** *584* (2–3), 269-277.

32. Luches, P.; D'Addato, S.; Valeri, S.; Groppo, E.; Prestipino, C.; Lamberti, C.; Boscherini, F., *Phys. Rev. B* **2004,** *69* (4), 045412.

33. Flank, A. M.; Delaunay, R.; Lagarde, P.; Pompa, M.; Jupille, J., *Phys. Rev. B* **1996,** *53* (4), R1737-R1739.

34. Kresse, G.; Furthmüller, J., *Comp. Mater. Sci.* **1996,** *6* (1), 15-50.

35. Grimme, S., *J. Comput. Chem.* **2006,** *27* (15), 1787-1799.

36. Ehrlich, S.; Moellmann, J.; Reckien, W.; Bredow, T.; Grimme, S., *ChemPhysChem* **2011,** *12* (17), 3414-3420.

37. Grimme, S.; Antony, J.; Ehrlich, S.; Krieg, H., *J. Chem. Phys.* **2010,** *132* (15), 154104.

38. Ferrari, A. M.; Pacchioni, G., *J. Phys. Chem.* **1995,** *99* (46), 17010-17018.

39. Didier, F.; Jupille, J., *Surf. Sci.* **1994,** *314* (3), 378-384.

40. Lozovoi, A. Y.; Alavi, A.; Kohanoff, J.; Lynden-Bell, R. M., *J. Chem. Phys.* **2001,** *115* (4), 1661-1669.

41. Sushko, P. V.; Gavartin, J. L.; Shluger, A. L., *J. Phys. Chem. B* **2002,** *106*, 2269-2276.

42. Kantorovich, L. N.; Shluger, A. L.; Sushko, P. V.; Gunster, J.; Stracke, P.; Goodman, D. W.; Kempter, V., *Faraday Discuss.* **1999,** *114*, 173-194.

Table of contents graphic

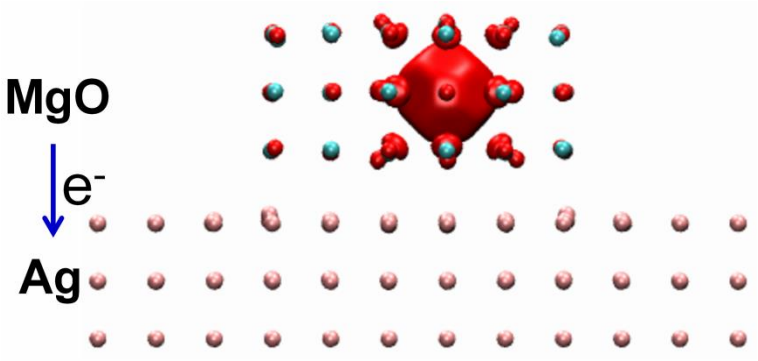

Table 1. Lattice parameter (Å), work function (eV), band gap (eV) and ionisation potential (eV) of Ag and MgO determined by different methods. Relevant theoretical values from previous studies are given in brackets for reference.

Material	Method	Lattice Parameter	Work function	
Ag	PBE	4.16 (4.147a)	4.36 (4.30d)	
	PBE0	- (4.142a)	4.29	
	Expt.	4.069a	4.38b	
Material	Method	Lattice Parameter	Band gap	IP
MgO	PBE	4.28 (4.258a)	4.36 (4.75a)	4.66
	PBE0	4.24 (4.211a)	7.04 (7.24a)	6.01
	Expt.	4.207a	7.7a	6.7c

[a] Ref. 24

[b] Ref. 7

[c] Ref. 42, for 2 nm thick MgO film

[d] Ref. 9, with PW91 functional

Table 2. Work function (ϕ), work function shift ($\Delta\phi$) and Schottky barrier height (E_{SB}) for MgO/Ag(001) interface calculated by different methods using the slab model. Relevant theoretical values from previous studies are given in brackets for reference. All energies are in eV.

	method	ϕ	$\Delta\phi$	E_{SB}
MgO(3L)/Ag(001)	PBE	2.62 (3.12a)	1.74 (1.27a)	2.35
	PBE0(MgO)/PBE(Ag)	2.57	1.78	3.58
	PBE0	2.57	1.78	3.67
	Expt.	3.05±0.05b	1.4b	3.85b

[a] Ref. 10, based on plane wave PW91 calculations

[b] Ref. 7

Table 3. Work function (ϕ, in eV), work function shift ($\Delta\phi$, in eV) and average interface Ag-O distance ($d_{Ag\text{-}O}$, in Å) for Ag(001) surface with different coverages by MgO clusters.

coverage	ϕ	$\Delta\phi$	$d_{Ag\text{-}O}$
17%	3.36	1.00	2.50
34%	3.19	1.17	2.53
56%	2.86	1.49	2.54
100%	2.57	1.78	2.58

Table 4. Relative stabilities of F centers at different sites of an MgO cluster supported on Ag(001). Two different sizes of MgO cluster were considered to check the finite size effect of our cluster model. Relative energies were calculated with respect to the most stable charge state of each case. We did not consider a kink site for an MgO(3x3) cluster due to its small size which cannot accommodate such a defect. All energies are in eV.

Size	Type	Terrace	Corner	Edge	Step corner	Kink
3x3	F^0	0.18	0.02	0	0.20	-
	F^+	0	0	0.05	0	-
	F^{2+}	0.31	0.62	0.63	0.57	-
5x5	F^0	0	0	0	0.09	0.42
	F^+	0.05	0.09	0.16	0	0
	F^{2+}	0.64	1.03	1.05	0.52	0.25

Table 5. Shift of the Ag work function ($\Delta\phi$, in eV) induced by MgO slab with surface F centers. MgO(4x4) and MgO(6x6) represent a 4x4 and a 6x6 slab, respectively. The relative shift of the Ag work function ($\Delta\phi_{rel}$, in eV) is defined with respect to the shift of the Ag work function induced by a perfect 4x4 MgO slab.

MgO(3L)/Ag(001)	Type	$\Delta\phi$	$\Delta\phi_{rel}$
MgO(4x4)	F^0	1.79	+0.01
	F^+	2.50	+0.71
	F^{2+}	3.00	+1.21
MgO(6x6)	F^0	1.78	+0.00
	F^+	2.15	+0.37
	F^{2+}	2.46	+0.67

Table 6. Shift of Ag work function (in eV) caused by F centers with different charge states located at different positions in a 3x3 MgO cluster on a 6x6 Ag(001) slab, which corresponds to a coverage of 17%.

Type	Terrace	Bulk	Edge	Corner
F^0	0.92	0.98	0.90	1.03
F^+	1.41	1.46	1.38	1.45
F^{2+}	1.85	1.86	1.75	1.76

Figure 1. (a) Side view of MgO/Ag(001) interface structure. (b) Top view of MgO/Ag(001) interface structure. A 3x3 MgO cluster on top of a 6x6 Ag slab is shown. Color code: green indicates Mg, red indicates O, and light blue indicates Ag atoms.

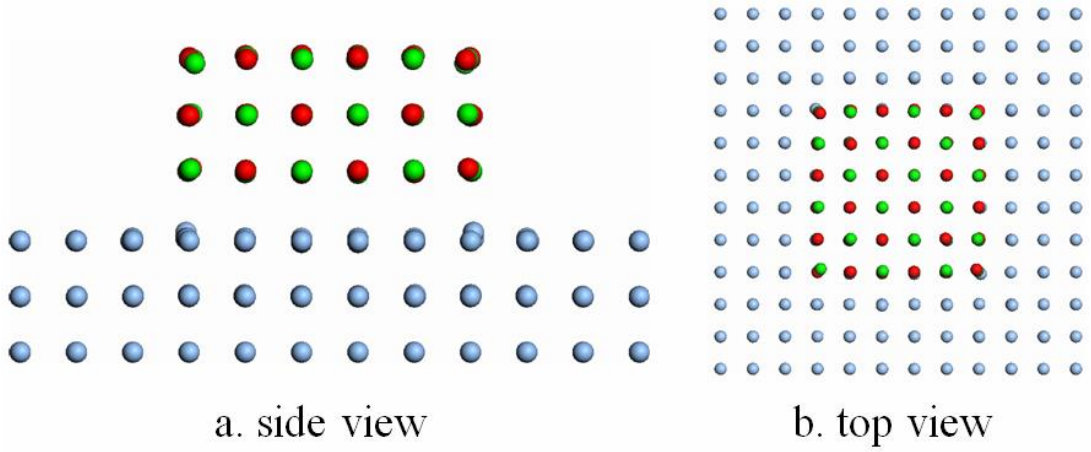

Figure 2. (a) Potential energy surface of an F center in MgO(4L)/Ag(001). F centers at different distances from the Ag(001) substrate were considered: an F center in the surface (black), second (red) and third (blue) layers of MgO cluster. Relative energies, ΔE, are defined with respect to the energy of the F^0 center in the surface layer of MgO cluster. (b) Schematic of geometry relaxations of oxygen (red sphere) and magnesium (cyan sphere) ions around an F center in different charge states. The directions of arrows follow the order of $F^0 \rightarrow F^+ \rightarrow F^{2+}$.

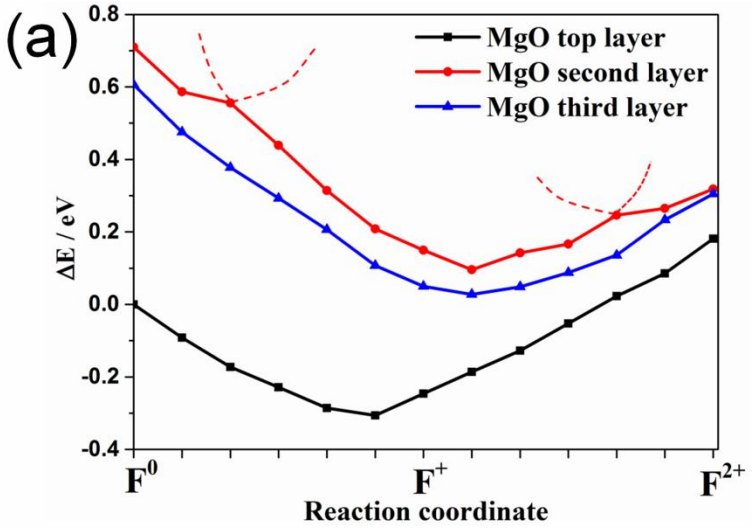

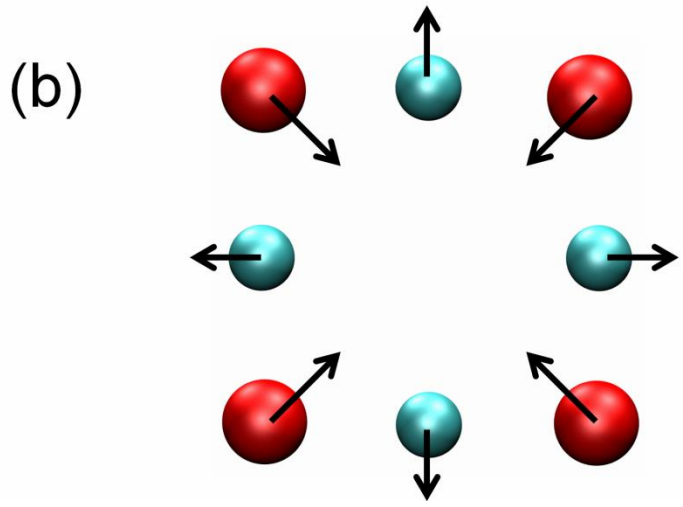

Figure 3. Isosurfaces (side view) of electron density differences between MgO(3L)/Ag(001) interface and the two separated components, bare Ag(001) slab and unsupported MgO slab (with or without point defect): (a) perfect, (b) with a surface F^0 center, (c) with a surface F^+ center, and (d) with a surface F^{2+} center. Blue and red surfaces indicate increase and decrease in electron density in the interface compared to the isolated constituents, respectively. A density value of 0.02 electron/bohr^3 is used for all isosurfaces.

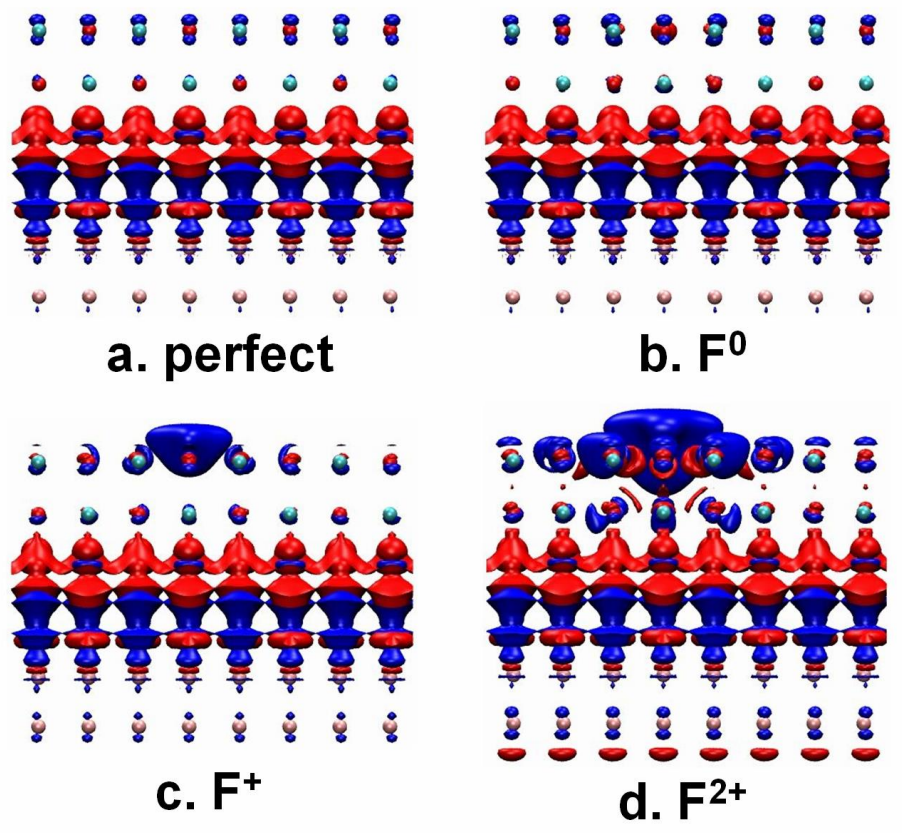

Figure 4. F centers (blue spheres) at different positions in MgO cluster considered in the calculations, including edge, corner, terrace, step corner, kink (top layer), and bulk (second layer, not shown).

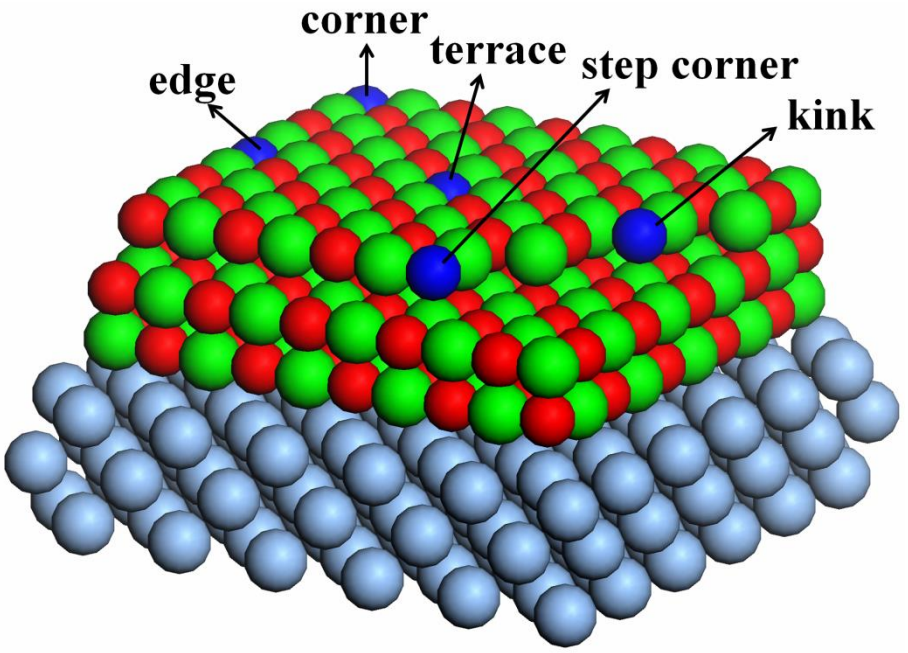

Figure 5. (a) The calculated one-electron energy levels of F^0 (red lines) and F^+ (light blue lines) centers at different positions in a 5x5 MgO cluster supported on a 6x6 Ag(001) slab. Solid and dashed lines denote occupied and unoccupied states related to F centers, respectively, and double solid lines denote occupied states related to under-coordinated oxygen atoms at corner sites. All energies are in eV. (b) Isosurfaces of a Kohn-Sham orbital showing occupied electronic state associated with under-coordinated oxygen atoms at corner sites in a 5x5 MgO cluster supported on a 6x6 Ag(001) slab. This state has one-electron energy level which is 2.3~2.6 eV below Ag Fermi level. Only part of the MgO cluster in Figure 4 is shown here. Blue and red surfaces indicate Kohn-Sham orbital with positive and negative coefficients, respectively. Red, cyan and pink spheres indicate oxygen, magnesium and silver atoms, respectively. A contour value of 0.02 $bohr^{-3/2}$ is used for all isosurfaces.